Thermally activated spin fluctuations in stoichiometric LiCoO$_2$ clarified by electron paramagnetic resonance and muon-spin rotation and relaxation measurements

Kazuhiko Mukai,[1,*] Yoshifumi Aoki,[1] Daniel Andreica,[2] Alex Amato,[3] Isao Watanabe,[4] Sean R. Giblin,[5] and Jun Sugiyama[1]

[1]*Toyota Central Research and Development Laboratories, Inc., 41-1 Yokomichi, Nagakute, Aichi 480-1192, Japan*
[2]*Faculty of Physics, Babes-Bolyai University, 400084 Cluj-Napoca, Romania*
[3]*Laboratory for Muon Spin Spectroscopy, Paul Scherrer Institut (PSI), Villigen, CH-5232, Switzerland*
[4]*Advanced Meson Science Laboratory, The Institute of Physical and Chemical Research (RIKEN), 2-1 Hirosawa, Wako, Saitama 351-0198, Japan*
[5]*School of Physics and Astronomy, Cardiff University, Queens Building, The Parade, Cardiff, CF24 3AA, United Kingdom*

Lithium cobalt dioxide (LiCoO$_2$) belongs to a family of layered CoO$_2$-based materials and has considerable interests in both fundamental physics and technological applications in lithium-ion batteries. We report the results of structural, electrochemical, magnetic susceptibility (χ), electron paramagnetic resonance (EPR), and muon-spin rotation and relaxation (μSR) measurements on powder Li$_{x0}$CoO$_2$ samples, where the nominal Li/Co ratios (x_0) were 0.95, 1.00, 1.02, 1.05, and 1.10, respectively. Structural, electrochemical, and χ measurements suggested that the sample with $x_0 = 1.02$ is very close to single stoichiometric LiCoO$_2$ (ST-LCO) phase and that the Co ions in the $x_0 = 1.02$ sample are in a nonmagnetic low-spin state with $S = 0$ (t_{2g}^6). However, both EPR and μSR revealed that the $x_0 = 1.02$ (ST-LCO) sample includes a large amount of nonordered magnetic phase in the temperature (T) range between 100 and 500 K. The volume fraction of such magnetic phase was found to be $\sim$45 vol% at 300 K by μSR, indicating an intrinsic bulk feature for ST-LCO. In fact, structural and photoelectron spectroscopic analyses clearly excluded the possibility that the nonordered magnetism is caused by impurities, defects, or surfaces. Because EPR and μSR sense static and dynamic nature of local magnetic environments, we concluded that Co spins in ST-LCO are fluctuating in the EPR and μSR time-windows. We also proposed possible origins of such nonordered magnetism, that is, a spin-state transition and charge disproportionation.

I. INTRODUCTION

Lithium cobalt dioxide LiCoO$_2$ (LCO) is still at the forefront of the positive electrode materials for lithium-ion batteries (LIBs) [1], despite strenuous efforts to find alternative materials. Stoichiometric (ST-)LCO possesses a layered structure with space group of $R\bar{3}m$, in which the Li$^+$ and Co^{3+} ions occupy the octahedral 3b and 3a sites, respectively, in a cubic close-packed array of O^{2-} ions. When the Li$^+$ ions are extracted from ST-LCO, the crystal structure of Li$_{1-y}$CoO$_2$ is known to change with y at ambient temperature (T) [2]. As y increases from $\sim$0.44, the rhombohedral ($R\bar{3}m$) phase transforms into a monoclinic ($C2/m$) phase, and then the $R\bar{3}m$ phase appears again above $\sim$0.5 [2]. Since these structural transformations with y cause particle fracture and degrade the cyclability of LIB, a lithium over-ST (OST-)LCO, for which the nominal Li/Co ratio (x_0) is larger than $\sim$1.05, is currently used in commercial LIBs to suppress such structural transformations [3,4].

A chemical formula of (Li)$_{3b}$[Li$_\delta$Co$_{1-3\delta}^{3+(LS)}$Co$_{2\delta}^{3+(IS)}$]$_{3a}$O$_{2-\delta}$ has been proposed for OST-LCO on the basis of magnetic susceptibility (χ) and ^{7}Li-nuclear magnetic resonance (NMR) measurements, where the LS and IS represent a low spin (LS) state with $S = 0$ (t_{2g}^6) and an intermediate spin (IS) state with $S = 1$ ($t_{2g}^5 e_g^1$), respectively, and δ is the amount of Li$^+$ ions at the 3a (Co) site [5,6]. Here $x_0 = (1 + \delta)/(1 - \delta)$ if we ignore evaporation of the Li atoms during the synthesis

at high temperatures. Since the Co^{3+} ions in ST-LCO are reported to be in the LS state with $S = 0$ (t_{2g}^6), according to the χ [7] and ^{7}Li-NMR [8,9] results, the magnetism of LCO would vary with x_0. Indeed, χ measurements below 150 K indicated that the effective magnetic moment ($\mu_{\rm eff}$) per Co ion increases with x_0 [10]. However, the magnetic nature of LCO is still not fully understood, as discussed by Chernova *et al.* [11]. Specifically, muon-spin rotation and relaxation (μSR) experiments on ST-LCO indicated the appearance of an oscillatory signal with $\sim$10 vol% below $\sim$30 K, owing to the formation of antiferromagnetic (AF) order [12,13]. Ménétrier *et al.* [14] and Artemenko *et al.* [15] also showed that even a very ST (VST-)LCO, which is prepared by using a high-purity Co$_3$O$_4$ compound, exhibits a Curie-Weiss paramagnetic (PM) behavior due to localized magnetic moments below $\sim$30 K, as revealed by electron paramagnetic resonance (EPR) measurements. Artemenko *et al.* [15] proposed, however, that a PM center consisting of Li$^+$-O$^-$ at grain boundaries and/or surfaces is the origin of these localized magnetic moments. For OST-LCO, Hertz *et al.* [10] reported that the excess lithium ions in the 3a (Co) site produce the Co^{4+} ions with a high spin (HS) state with $S = 5/2$ ($t_{2g}^3 e_g^2$).

Magnetic properties are generally sensitive to structural defects, oxygen deficiencies, and impurities in a sample as compared with a conventional x-ray diffraction (XRD) technique. Magnetic information, therefore, often plays a crucial role in understanding the complex structural nature of LIB materials, leading to insights into how to improve LIB performance. From the viewpoint of condensed matter physics, magnetism of LIB materials is a subject of considerable

*e1089@mosk.tytlabs.co.jp

interest because the electrochemical delithiation/lithiation reaction provides unusual oxidation states and electronic configurations of transition metal ions. In the case of LCO, the Co ions form a two-dimensional triangular lattice by connection of edge-sharing CoO_6 octahedra, resulting in an additional contribution from geometrical frustration to the magnetic nature. To shed more light on the magnetic properties of LCO, here we report the results of systematic χ, EPR, and μSR measurements of LCO. Note that the three techniques cover a wide range of time windows. Furthermore, the samples were prepared by a conventional solid-state reaction technique with x_0 ranging between 0.50 and 1.10 to clarify the effects of lithium poor and over stoichiometry on the magnetism. Since the representation $Li(Li_\delta Co_{1-\delta})O_{2-\delta}$ can be used only for ST- and OST-LCO, we hereafter use the x_0 value to describe the present LCO samples. As a result, besides the AF order below 30 K, we have found the presence of spin fluctuations in ST-LCO at temperatures between 100 and 500 K and confirmed that such spin fluctuations are not due to impurities but due to an intrinsic nature of ST-LCO. In this paper, we first describe the sample characterization in the Sec. III and then discuss the results of magnetic measurements in the Sec. IV.

II. EXPERIMENTAL

Powder samples of LCO were prepared by a solid-state reaction technique, as reported previously [4,13]. Co_3O_4 powder was first synthesized by heating CoO powder (99.7%, Kojyundo Chemical Lab. Co. Ltd.) at 1023 K for 12 h in air. Then, a reaction mixture of Li_2CO_3 (99%, Wako Pure Chemical Industries, Ltd.) and Co_3O_4 was well mixed with a pestle and mortar and pressed into a pellet 23 mm in diameter and ∼5 mm in thickness. The x_0 value (= Li/Co) of the mixture was 0.50, 0.75, 0.85, 0.90, 0.95, 1.00, 1.02, 1.05, or 1.10. The pellets were heated at 1173 K for 12 h in air and cooled down to ambient temperature at a rate of 5 K·min^{-1}. The obtained powders were characterized by powder XRD measurements with Fe-Kα radiation (D8 ADVANCE, Bruker AXS, Inc.) and scanning electron microscopy (SEM, S-3600N, Hitachi High-Technologies Co. Ltd.) analyses. An x-ray photoelectron spectroscopy (XPS, Quantera SXM, ULVAC-PHI, Inc.) analysis was conducted using monochromatic Al-Kα radiation. From now on, the $x_0 = nnn$ sample is called LCO($x_0 = nnn$) to avoid confusion between nominal composition and real composition in the sample.

The electrochemical reactivity of LCO($0.95 \leq x_0 \leq 1.10$)s was examined in a nonaqueous lithium cell. Polyvinylidene fluoride (PVdF) dissolved in an N-methyl-2-pyrrolidone solution was used as a binder when preparing the electrode. The resulting black viscous slurry, consisting of 88 wt% LCO powder, 6 wt% acetylene black (AB), and 6 wt% PVdF, was cast on an aluminum foil with a blade. The electrode ($\varphi = 16$ mm) was dried under vacuum at 393 K for 12 h. A lithium metal sheet pressed on a stainless steel plate ($\varphi = 19$ mm) was used as a counter electrode. Two sheets of a porous polyethylene membrane (TonenGeneral Sekiyu K. K.) were used as the separator. The electrolyte was 1 M $LiPF_6$ dissolved in an ethylene carbonate (EC)/dimethyl carbonate (DEC) (EC/DEC = 1/1 by volume ratio) solution (Kishida Chemical Co. Ltd.). The charge and discharge cycle test was performed in the voltage range between 3 and 4.2 V with a current density of 0.25 mA·cm^{-2} at 298 K.

Magnetic susceptibility (χ) was measured using a superconducting quantum interference device (SQUID) magnetometer (MPMS, Quantum Design, Inc.) in the T range between 5 and 400 K with a magnetic field (H) of 10 kOe. The sample was packed between two sheets of aluminum foil and then attached to the sample rod with copper wire. X-band (9.6 GHz) EPR spectra were recorded by an ESP300E spectrometer (Bruker BioSpin K. K.) in the T range between 100 and 400 K with a microwave field (H_1) of 1 Oe and a microwave power of 3.2 mW. For LCO($x_0 = 1.02$), the EPR spectra were also measured at 300 K in the H_1 range between 1 and 30 Oe to obtain a spin–lattice relaxation time T_1 and a spin–spin relaxation time T_2. Furthermore, X-band pulsed EPR measurements were conducted for LCO($x_0 = 1.02$) by an Elexsys E580 spectrometer (Bruker BioSpin K. K.). The gyromagnetic (g) factor of Co ions was determined with respect to a MnO/MgO standard.

Muon-spin rotation and relaxation (μSR) spectra were recorded in the T range between 2 and 300 K using the General Purpose Surface-muon Spectrometer (GPS) at the Paul Scherrer Institut (PSI) in Switzerland and in the T range between 150 and 500 K on the muon spectrometer (EMU) at ISIS of Rutherford Appleton Laboratory (RAL) in the United Kingdom and on ARGUS at the RIKEN-RAL Muon Facility at RAL. Muon is an elementary particle with spin 1/2 and a gyromagnetic ratio $\gamma_\mu/2\pi = 13.554$ kHz/Oe. When ∼100% spin-polarized muons are injected into a sample, the muon-spin precesses due to the local internal magnetic field (H_{int}) at the muon site. The muon decays with a mean lifetime of 2.2 μs into a positron, which is preferentially emitted along the muon-spin direction, and two neutrinos. By collecting the positrons as a function of time (t), one can construct the t dependence of the muon-spin polarization [$A_0 P(t)$], where A_0 is the initial asymmetry and $P(t)$ is the polarization function [16]. If there are multiple muon sites with different H_{int}s, the $A_0 P(t)$ function is given by a sum of the different spin polarization functions; that is, $A_0 P(t) = \Sigma A_i P_i(t)$. When such multiple muon sites are caused by the coexistence of multiple phases in the sample, A_i/A_0 corresponds to the volume fraction of the ith phase. On the contrary, when all the muon sites are crystallographically equivalent but magnetically different, A_i/A_0 indicates the fraction of the muon sites with H_{int}^i to all of the sites. Muon-spin rotation and relaxation is very sensitive to H_{int} ranging from 0.1 Oe to 100 kOe caused by the nuclear and electronic magnetic moments [16]. Furthermore, it can detect magnetic fluctuation rates ranging between 10^4 and 10^{12} Hz, which bridges the gap between the time windows of NMR (10^{-2}–10^4 Hz) and neutron scattering (10^8–10^{13} Hz) [16]. The muon beams are distinguished by their time structure. Continuous muon beam facilities, such as PSI and TRIUMF in Canada, are suitable for the detection of large magnetic fields and fast relaxing signals, while pulsed muon beam facilities, such as RAL and the Japan Proton Accelerator Research Complex (J-PARC), are ideal for studying relatively slowly relaxing behaviors.

A delithiated $Li_{1-y}CoO_2$ sample with $y = 0.05$ for the μSR measurements was prepared by electrochemical reaction in a nonaqueous Li cell using the LCO($x_0 = 1.02$) sample.
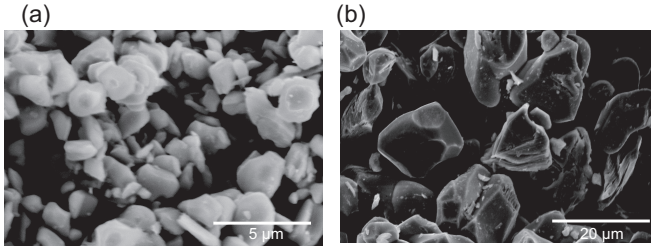
FIG. 1. SEM images for the (a) LCO($x_0 = 1.02$) and (b) LCO ($x_0 = 1.10$) samples.

To avoid the signals from AB and PVdF, the electrode was made only from LCO($x_0 = 1.02$) powder. The Li/Co ratio after the μSR measurements was determined to be 0.96 by inductively coupled plasma atomic-emission spectroscopy (ICP-AES) analysis (CIROS, Rigaku Co. Ltd.). The details of the experimental setup and techniques for the μSR measurements are described elsewhere [12,13].

III. SAMPLE CHARCTERIZATION

We first describe the morphology, crystal structure, and electrochemical properties of the present samples, which are essential to the precise determination of the stoichiometry and/or lithium over-stoichiometry of LCO. Particularly, although the electrochemical measurements are unlikely common in the condensed-matter physics world, electrochemical properties are known to be very sensitive to the composition and homogeneity of a sample [1–3,17]. This is because the voltage for the extraction (insertion) of Li$^+$ ions from (into) the lattice strongly depends on the structure and composition of the compound. As a result, from the charge/discharge curve, which corresponds to the extraction/insertion of Li$^+$ ions from/into the lattice, one can evaluate the structure, composition, and homogeneity of the sample.

Figure 1 shows the SEM images of (a) LCO($x_0 = 1.02$) and (b) LCO($x_0 = 1.10$). The particle morphology and average size of a primary particle (d_{ave}) for LCO($x_0 \leq 1.02$)s differ greatly from those for LCO($x_0 \geq 1.05$)s. The particles with $d_{ave} \approx 2$ μm are agglomerated together for LCO($x_0 = 1.02$), while those with $d_{ave} \approx 15$ μm appear to be separate each other for LCO($x_0 = 1.10$). This is probably because the excess Li$_2$CO$_3$ acts as a flux medium during synthesis [3,6]. Note that several particles in LCO($x_0 = 1.02$) have a hexagonal shape—similar to that for single-crystal LCO [18]—owing to anisotropic crystal growth along the [00l] direction.

XRD measurements showed that the starting material, Co$_3$O$_4$, remains in LCO($x_0 \leq 0.95$)s (see Supplemental Material 1 [19]), but the majority of the sample has a layered structure with the $R\bar{3}m$ symmetry. If we assume that LCO($x_0 < 1.00$)s are a mixture of ST-LCO and Co$_3$O$_4$, the weight fraction of the Co$_3$O$_4$ phase, W(Co$_3$O$_4$), is calculated by

$$W(\text{Co}_3\text{O}_4)$$
$$= \frac{(1 - x_0) \times M(\text{Co}_3\text{O}_4) \times 1/3}{x_0 \times M(\text{LiCoO}_2) + (1 - x_0) \times M(\text{Co}_3\text{O}_4) \times 1/3}, \quad (1)$$

where M(LiCoO$_2$) and M(Co$_3$O$_4$) are the molecular weights of LiCoO$_2$ and Co$_3$O$_4$, respectively. In fact, the W(Co$_3$O$_4$)

value estimated by a Rietveld analysis with RIETAN-2000 [20] decreases linearly with x_0; for instance, W(Co$_3$O$_4$) = 5.4(1) wt% for LCO($x_0 = 0.95$) (see Supplemental Material 2 [19]). Hence, the $R\bar{3}m$ phase in the LCO($x_0 < 1$) sample can be assigned to ST-LCO. This is significantly different from LiNiO$_2$, which is isostructural with LCO; a rock-salt phase, (Li$_{1-z}$Ni$_z$)$_{3b}$(Ni)$_{3a}$O$_2$, rather than ST (Li)$_{3b}$(Ni)$_{3a}$O$_2$, is easily formed when the initial Li/Ni ratio is less than 1 [21].

For LCO($x_0 \geq 1.00$)s, the XRD patterns are identified as single phase with the $R\bar{3}m$ symmetry (see Supplemental Material 1) [19]. We tried to obtain W(Co$_3$O$_4$) for LCO($x_0 \geq 1.00$)s; however, even for the XRD pattern measured at the synchrotron radiation facility, we could not determine those values due to the lack of XRD lines from the Co$_3$O$_4$ phase [4]. Thus, from the viewpoint of XRD measurements, the LCO($x_0 \geq 1.00$) samples are free from the Co$_3$O$_4$ phase. In addition, since the lattice parameters in the hexagonal setting are almost independent of x_0 ($a_h = 2.813$ Å and $c_h = 14.043$ Å; see Supplemental Material 3 [19]), the crystal structure of LCO is not sensitive to x_0 when $x_0 \geq 1.00$.

Figure 2 shows the charge and discharge curves of the Li/LCO cells to display the correlation between x_0 and the electrochemical properties for (a) LCO($x_0 = 0.95$), (b)
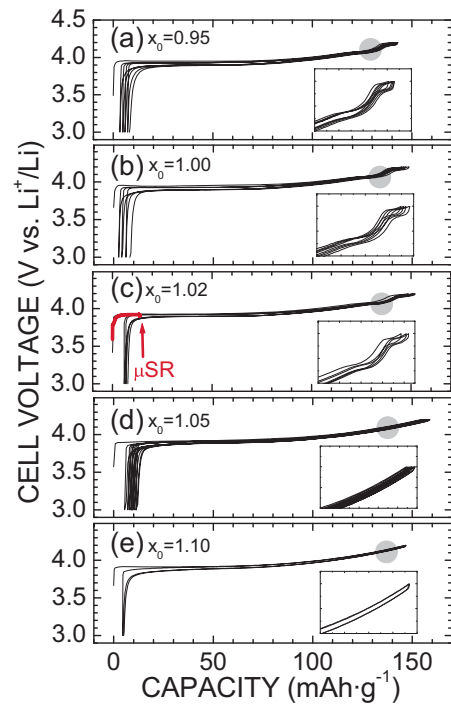
FIG. 2. (Color online) Charge and discharge curves for the Li/LCO cells with (a) LCO($x_0 = 0.95$), (b) LCO($x_0 = 1.00$), (c) LCO($x_0 = 1.02$), (d) LCO($x_0 = 1.05$), and (e) LCO($x_0 = 1.10$). The cells were operated in the voltage range between 3 and 4.2 V with a current density of 0.25 mA·cm^{-2} at 298 K. Inset shows enlarged charge and discharge curves at ~4.1 V. The change in the charge and discharge curves at ~4.1 V suggests the structural change between the rhombohedral ($R\bar{3}m$) and monoclinic ($C2/m$) phases, which is a characteristic of stoichiometric LiCoO$_2$. The red line in (c) indicates the charge curve for the μSR measurements on the delithiated Li$_{1-y}$CoO$_2$ sample with $y = 0.05$.

LCO($x_0 = 1.00$), (c) LCO($x_0 = 1.02$), (d) LCO($x_0 = 1.05$), and (e) LCO($x_0 = 1.10$). For LCO($x_0 = 0.95$), the cell voltage (V_{cell}) is almost constant (~ 3.95 V) up to the capacity $Q \approx 70$ mAh$\cdot$g^{-1} and then monotonically increases with Q. The initial discharge capacity (Q_{dis}) is 147 mAh$\cdot$g^{-1}. A small change in the $V_{cell}(Q)$ curve is clearly observed around 4.1 V [see inset in Fig. 2(a)]. This corresponds to the structural change between the $R\bar{3}m$ and $C/2m$ phases, which is known to be a characteristic feature for ST-LCO [2–6]. Therefore, the electrochemical measurements confirm the presence of the ST-LCO phase in LCO($x_0 = 0.95$), which is consistent with the result of the XRD measurements. For LCO($x_0 = 1.00$) and LCO($x_0 = 1.02$), the charge and discharge curves are similar to those for LCO($x_0 = 0.95$). On the contrary, such a small change in the $V_{cell}(Q)$ curve is no longer observed for LCO($x_0 = 1.05$) and LCO($x_0 = 1.10$), suggesting that the crystal structure maintains the $R\bar{3}m$ symmetry in the whole V_{cell} range measured. By comparing these results with the previous electrochemical studies on LCO [2–6], the electrochemical properties for LCO($x_0 \leq 1.02$)s are caused by ST-LCO, whereas those for LCO($x_0 = 1.05$) and LCO($x_0 = 1.10$) by OST-LCO. In other words, there is a clear phase boundary between ST-LCO and OST-LCO at $1.02 < x_0 \leq 1.05$.

Considering the results of morphology observation and structural and electrochemical analyses, it is found that LCO($x_0 = 1.02$) is almost a single phase of ST-LCO. That is, the amount of a possible impurity phase Co_3O_4 is below the detectable range of XRD (below 0.1 wt%).

IV. RESULTS AND DISCUSSION

A. Magnetic susceptibility

Figure 3(a) shows the T dependence of χ for LCO($0.95 \leq x_0 \leq 1.10$)s measured with a field-cooling protocol with $H = 10$ kOe. The measured magnetization data were corrected by subtracting the contributions from the aluminum foil and copper wire and were converted into molar χ. For LCO($x_0 = 0.95$), as T decreases from 400 K to ~ 50 K, χ gradually increases and then shows a cusp at ~ 35 K [inset in Fig. 3(a)], finally increasing rapidly as T decreases further. Since the Rietveld analysis suggested that $W(Co_3O_4) = 5.2(2)$ wt% in LCO($x_0 = 0.95$) [19], the cusp around 35 K is attributed to the AF transition of the Co_3O_4 phase ($T_N = 35$ K) [22]. For LCO($x_0 = 1.00$) and LCO($x_0 = 1.02$), χ is almost T independent down to ~ 50 K. This is consistent with previous works [7–9], which showed that the Co^{3+} ions in ST-LCO are in the LS state with $S = 0$ (t_{2g}^6). For LCO($x_0 = 1.05$) and LCO($x_0 = 1.10$), χ rapidly increases with decreasing T, particularly below ~ 50 K. Such a Curie-Weiss behavior indicates the presence of localized moments in the sample. In a PM state, a Curie-Weiss formula is represented by

$$\chi = \frac{N\mu_{eff}^2}{3k_B(T - \Theta_p)} + \chi_0, \quad (2)$$

where N is the number density of Co ions, k_B is the Boltzmann's constant, T is the absolute temperature, Θ_p is the Weiss temperature, and χ_0 is the T independent susceptibility.

Figure 3(b) shows the observed μ_{eff}(μ_{eff}^{obs}) for LCO($0.95 \leq x_0 \leq 1.10$)s obtained by fitting the $\chi(T)$ curve in the T range
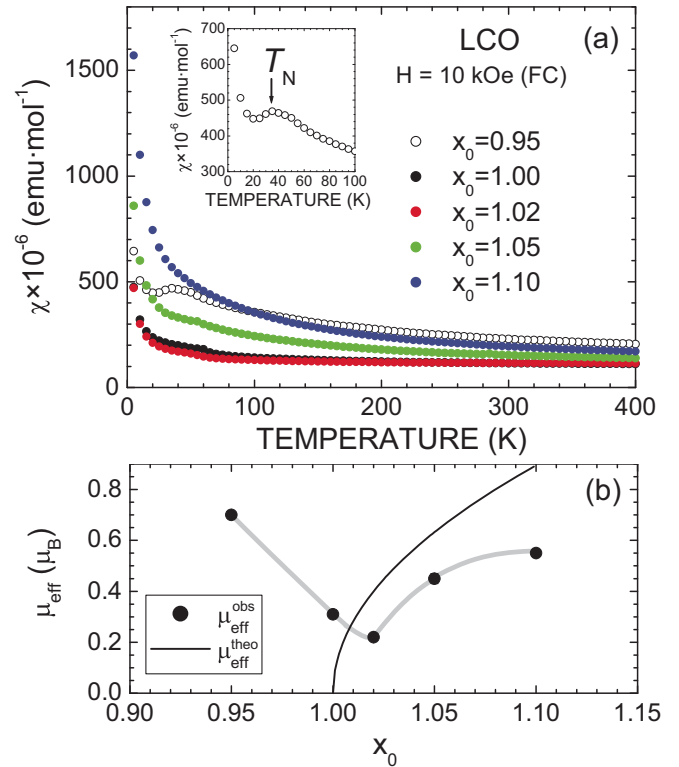
FIG. 3. (Color online) (a) Temperature dependence of the magnetic susceptibility (χ) for the LCO($x_0 = 0.95$), LCO($x_0 = 1.00$), LCO($x_0 = 1.02$), LCO($x_0 = 1.05$), and LCO($x_0 = 1.10$) samples. χ was measured with a field-cooling protocol with $H = 10$ kOe. The background magnetization, which consists of that from two sheets of aluminum foil and a copper wire, was subtracted from the raw magnetization. T_N ($= 35$ K) is the antiferromagnetic transition temperature for Co_3O_4. (b) The x_0 dependence of the observed effective magnetic moment per Co ion, μ_{eff}^{obs}. The solid line represents the theoretical effective magnetic moment per Co ion, μ_{eff}^{theo}, calculated by Eq. (3).

between 100 and 400 K with Eq. (2). Table I summarizes the estimated Curie-Weiss parameters, namely, μ_{eff}^{obs}, Θ_p, and χ_0. As x_0 increases from 0.95, μ_{eff}^{obs} decreases monotonically up to $x_0 = 1.02$ and then increases slowly with changing the slope ($d\mu_{eff}^{obs}/dx_0$). As described in the Introduction, Levasseur *et al.* [5,6] proposed that the Co^{3+} ions for the OST-LCO compounds are partially in the IS state with $S = 1$ ($t_{2g}^5 e_g^1$). Assuming that the $Co^{3+(IS)}$ ions with $S = 1$ exist in the LCO samples with $x_0 > 1.00$, a spin-only value of μ_{eff}(μ_{eff}^{theo}) for LCO is predicted as

$$\mu_{eff}^{theo} = g\sqrt{S(S+1) \times \frac{2\delta}{1-\delta}} \quad \left(\delta = \frac{x_0 - 1}{x_0 + 1}\right). \quad (3)$$

As seen in Fig. 3(b) and Table I, μ_{eff}^{theo} is larger than μ_{eff}^{obs} by 0.2–0.4 μ_B at $x_0 > 1.00$. However, the $\mu_{eff}^{theo}(x_0)$ curve is almost identical to the $\mu_{eff}^{obs}(x_0)$ curve if it shifts by 0.02 toward the higher x_0 side. Therefore, such a shift is reasonably caused by evaporation of Li atoms during the high T synthesis.

Note the small cusp at around 60 K in the $\chi(T)$ curve for LCO($x_0 = 1.00$), LCO($x_0 = 1.02$), and LCO($x_0 = 1.05$). Such cusp has been usually assigned as the PM behavior of O_2 in a sample space [6]. However, we wish to point out the

TABLE I. The observed effective magnetic moment per Co ion, $\mu_{\text{eff}}^{\text{obs}}$, Weiss temperature Θ_p, temperature-independent susceptibility χ_0, the theoretical effective magnetic moment per Co ion, $\mu_{\text{eff}}^{\text{theo}}$, and the χ value at 300 K for the LCO($0.95 \leq x_0 \leq 1.10$) samples.

x_0	$\mu_{\text{eff}}^{\text{obs}}(\mu_B)$	$\Theta_p(K)$	χ_0 $(10^{-6} \times$ emu $\cdot$ mol$^{-1})$	$\mu_{\text{eff}}^{\text{theo}}(\mu_B)$[a]	χ at 300 K $(10^{-6} \times$ emu $\cdot$ mol$^{-1})$
0.95	0.70(2)	$-118(2)$	132(1)	$-$	230
1.00	0.31(1)	$-93(5)$	110(6)	0	115
1.02	0.22(1)	$-76(6)$	100(5)	0.42	114
1.05	0.45(2)	$-52(2)$	101(9)	0.67	153
1.10	0.55(1)	$-37(1)$	105(4)	0.95	194

[a]$\mu_{\text{eff}}^{\text{theo}}$ is calculated by Eq. (3) and $g = 2.12$.

other explanation, because, as described in the Introduction, the previous μSR study on ST-LCO revealed the appearance of localized magnetic moments below 60 K. Namely, as T decreases from $\sim$60 K, a rapidly relaxing nonoscillatory signal appears in the spectrum, and then static AF order completes below $\sim$30 K, but its volume fraction is only $\sim$10 vol% [12,13]. The present μSR result of ST-LCO is described Sec. IVC.

From χ measurements on VST-LCO [14,15], Ménétrier *et al.* [14,15] proposed that χ is at ambient temperature, i.e., χ_0 is an indicator for verifying ST-LCO. This is because $\chi(300 \text{ K}) \sim 90 \times 10^{-6}$ emu·mol^{-1} for VST-LCO prepared using high purity Co_3O_4 (less than 10 mg/kg of Fe, Ni, or Cu and less than 20 mg/kg of Mn) but is 200×10^{-6} emu·mol^{-1} for ST-LCO prepared using standard Co_3O_4. Looking again at LCO($x_0 = 1.02$), which is identified as ST-LCO by electrochemical measurements [Fig. 2(c)], its $\chi(300 \text{ K})$ ($= 114 \times 10^{-6}$ emu·mol^{-1}) is the smallest among LCO($0.95 \leq x_0 \leq 1.10$)s. However, since $\chi(300 \text{ K})$ inevitably includes the Curie-Weiss contributions from the Co_3O_4 phase for LCO($x_0 < 1.00$)s and the IS state of Co^{3+} ions for LCO($x_0 > 1.00$)s, $\mu_{\text{eff}}^{\text{obs}}$ should be a more suitable parameter than χ_0 for verifying ST-LCO. Actually, as seen in Table I, as x_0 increases from 0.95, χ_0 decreases from $132(1) \times 10^{-6}$ emu·mol^{-1} to $110(6) \times 10^{-6}$ emu·mol^{-1} at $x_0 = 1.00$ and then levels off the constant value ($\sim$100 $\times 10^{-6}$ emu·mol^{-1}) until $x_0 = 1.10$. On the contrary, as shown in Fig. 3(b) and Table I, $\mu_{\text{eff}}^{\text{obs}}$ has a minimum at $x_0 = 1.02$ [0.22 (1) μ_B]. This means that the optimal x_0 for ST-LCO is 1.02 under the present synthesis condition, namely, the excess Li atoms ($0.02 = 1.02 - 1$) are consumed to compensate for the Li lost by evaporation during synthesis. We wish to emphasize again that LCO($x_0 = 1.02$) is almost a single ST-LCO phase, based on the structural, electrochemical, and magnetic measurements.

B. Electron paramagnetic resonance

In order to know the variation of the state of d electrons with x_0, Fig. 4 shows the EPR spectra for LCO($0.95 \leq x_0 \leq 1.10$)s at (a) 100 and (b) 300 K. If we assume that the Co^{3+} ions are in the LS state with $S = 0$ (t_{2g}^6), LCO($x_0 = 1.02$), for which all the Co ions are in a +3 state, should be EPR-inactive due to the lack of unpaired electrons. Nevertheless, an EPR signal is clearly observed at 100 K [Fig. 4(a)]. The g factor is calculated as 2.12(1) using the following relation:

$$h\nu_r = g\mu_B H_r, \quad (4)$$

where h is the Planck constant, ν_r is the resonance frequency, and H_r is the resonance field. The intensity of the EPR signal with $g = 2.12(1)$ is enhanced at 300 K [Fig. 4(b)] but is too small to be detected at 400 K (see Supplemental Material 4 [19]). The EPR signal also appears for the samples with $x_0 = 0.95$, 1.00, and 1.05 at 300 K. Although the intensity of the EPR signal is strongest for LCO($x_0 = 1.02$), both the g factor and EPR line width between the peaks (ΔH_{pp}) are independent of x_0 [Fig. 4(c)], confirming the common origin for the EPR signal in LCO($0.95 \leq x_0 \leq 1.10$)s.

Since the purity of the staring material CoO (or Co_3O_4) was $\sim$99.7%, all the LCO samples should include impurity phases, such as Fe, Ni, or Mn oxides. Moreover, one can naturally expect the EPR signals from the CoO or Co_3O_4
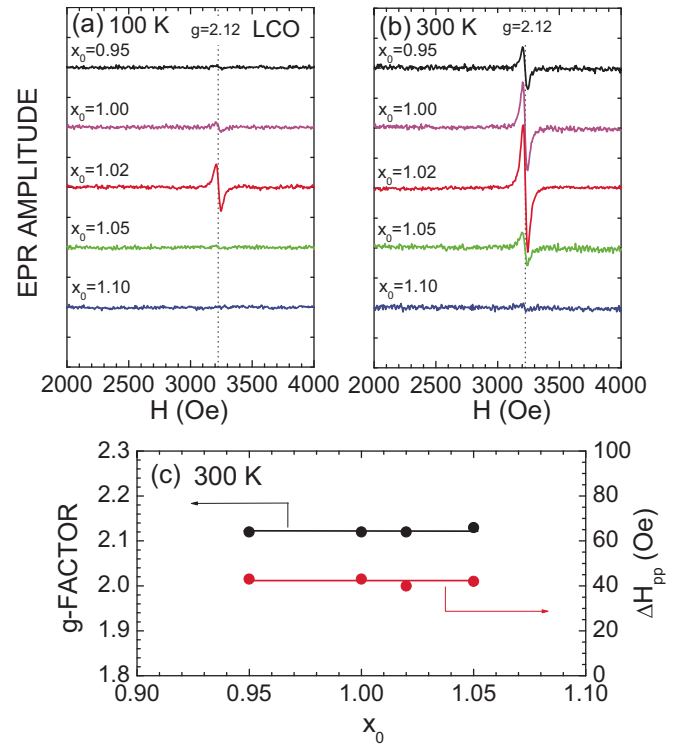
FIG. 4. (Color online) Electron paramagnetic resonance (EPR) spectra for the LCO($0.95 \leq x_0 \leq 1.10$) samples at (a) 100 and (b) 300 K. Vertical dotted lines correspond to the EPR signal with $g = 2.12$. (c) The x_0 dependence of the g factor and the EPR line width between the peaks (ΔH_{pp}) at 300 K.

phases. However, such impurities are most unlikely to be an origin of the EPR signal due to the following reasons.

First, the EPR signal with $g = 2.12$ was not observed for LCO($x_0 = 1.10$) at 100 and 300 K [Figs. 4(a) and 4(b)]. Second, the EPR signal was not observed for the pristine CoO at 300 K (see Supplemental Material 5 [19]). Finally, the Co_3O_4 phase is known to have a broad EPR signal with $g \approx 5$ at ambient temperature [15]. The EPR signal with $g = 2.12$ is, thus, considered as an intrinsic behavior for ST-LCO.

Interestingly, the EPR signal with $g = 2.12$ at ambient temperature has not been reported for either ST-LCO or OST-LCO. Although Artemenko *et al.* [15] reported an EPR signal with $g = 2.16$ for VST-LCO, probably due to the Li^+–O^- PM centers; such an EPR signal is observed only below ~ 30 K with $\Delta H_{pp} \approx 110$ Oe. Kim *et al.* [23] reported the EPR signal with $g \approx 2.16$ at ambient temperature for the compound prepared by a molten salt method with $x_0 = 7$. However, their LCO compound is most likely quite different from a typical ST-LCO and OST-LCO based on their electrochemical data, such as a large hysteresis between the charge and discharge curve and a small Q_{dis} value (<100 mAh·g^{-1}) in the voltage range between 2.8 and 4.2 V [23].

For LCO($x_0 = 1.02$), the absorption EPR spectra were well fitted by a Lorentzian function, suggesting a typical homogeneous resonance [24]. In other words, the energy absorbed from the microwave field is distributed to all the spins, and thermal equilibrium of the spin system is preserved through the resonance absorption. Thus, the spin–spin relaxation time (T_2) is determined using

$$T_2 = \frac{h}{2\sqrt{3}\pi g \mu_B \Delta H_{pp}} = \frac{1}{1.52 \times 10^7 g \Delta H_{pp}}. \quad (5)$$

Using the values of g [$=2.12(1)$] and ΔH_{pp} [$=42(1)$ Oe] in the T range between 100 and 300 K, T_2 is calculated as $7.4(1) \times 10^{-10}$ s. This value is faster by about two orders of magnitude than that for a typical radial compound 1,1-diphenyl-2-picrylhydrazyl (DPPH) at 300 K ($\sim 10^{-8}$ s) and is comparable to that for the Fe^{3+} ions in $Fe_2(SO_4)_3$ (6.3×10^{-10} s) [25]. On the contrary, the spin–lattice relaxation time (T_1) is usually given by

$$T_1 = \left(\frac{h}{2\pi g \mu_B}\right)^2 H_{1/2}^2 T_2, \quad (6)$$

where $H_{1/2}$ is the H_1 value that makes the saturated EPR intensity $1/2$. However, the EPR intensity with $g = 2.12$ at 300 K increases in proportion to H_1 until 30 Oe (see Supplemental Material 6 [19]). This suggests that T_1 is too fast to be determined by EPR measurements. We obtained the same conclusion by pulsed EPR (X-band) measurements at 300 K.

C. Muon-spin rotation and relaxation

In order to investigate the internal magnetic field more precisely, μSR spectra were recorded in the T range between 2 and 500 K for LCO($x_0 = 1.02$). Figure 5 shows the T dependence of the weak-transverse-field (wTF-) normalized asymmetry (N_{ATF}) for LCO($x_0 = 1.02$). Here, "weak" means that the applied magnetic field ($=50$ Oe) is significantly lower than any possible spontaneous H_{int}. The "transverse
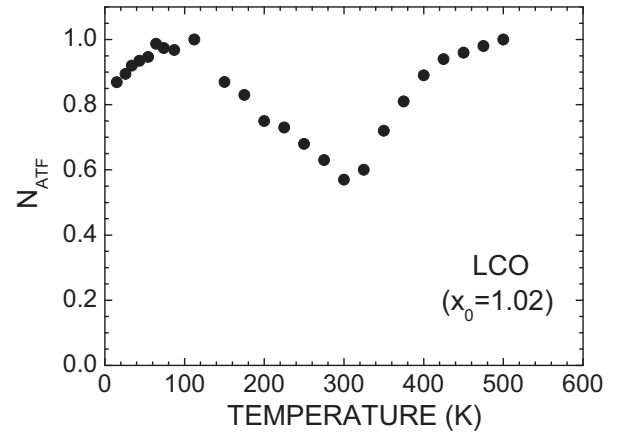
FIG. 5. Temperature (T) dependence of the normalized weak-transverse-field (wTF-) μSR asymmetry (N_{ATF}) for the LCO($x_0 = 1.02$) sample.

field" represents the field perpendicular to the initial muon-spin polarization. N_{ATF} roughly corresponds to the volume fraction of nonmagnetic phases in a sample. For instance, when $N_{ATF} = 0$, the whole volume of a sample is in a magnetic ordered/disordered state such as a ferromagnetic, AF, ferrimagnetic, spin-glass, or PM state with large localized moments. In contrast, when $N_{ATF} = 1$, the whole sample is in a nonmagnetic state with $H_{int} \ll$ wTF. According to the previous μSR study on ST-LCO [12,13], it was found that $N_{ATF} \approx 0.85$ at 2 K due to the formation of AF order. Such AF order is a characteristic feature for ST-LCO and is caused by either the charge disproportionation of $2Co^{3+} \rightarrow Co^{2+} + Co^{4+}$, the spin-state transition of $t_{2g}^6 \rightarrow t_{2g}^5 e_g^1$, or the surface magnetism [12,13]. As T increases from 2 K, N_{ATF} increases with T and reaches the maximum ($=1$) around 60 K, suggesting that the whole volume of the sample is in the nonmagnetic state at 60 K.

For the present work in the T range above 100 K, N_{ATF} monotonically decreases from 1 to ~ 0.55 with T up to 300 K, then gradually increases with further increasing T, and finally reaches the maximum again at 500 K. The T dependence of N_{ATF} above 100 K is consistent with the results of the EPR measurements for LCO($x_0 = 1.02$). That is, the EPR signal with $g = 2.12$ at 300 K was more remarkable than that at 100 K [Figs. 4(a) and 4(b)], but such a signal was absent at 400 K (see Supplemental Material 4 [19]). Since $N_{ATF} \approx 0.55$ at 300 K, ~ 45 vol% of the sample is not a typical nonmagnetic phase at 300 K.

Figure 6 shows the T dependence of the zero-field (ZF-) and longitudinal-field (LF-) μSR spectra for LCO($x_0 = 1.02$) at (a) 500, (b) 300, (c) 125, and (d) 2 K in the time domain below 10 μs. In order to clarify the existence/absence of static magnetic order in the sample, the ZF-μSR spectra in the time domain below 1 μs are also displayed at (e) 300 K, (f) 125 K, and (g) 2 K. The ZF-μSR spectrum at 500 K shows a typical Kubo–Toyabe (KT-)type [26] relaxation with a minimum at ~ 6 μs caused by the nuclear magnetic moments of the ^{6}Li (0.82 μ_N), ^{7}Li (3.26 μ_N), and ^{59}Co (4.63 μ_N) ions. This is consistent with the wTF-μSR result where $N_{ATF} \approx 1$ at 500 K (Fig. 5). The applied LF ($=5$ Oe) clearly reduces the
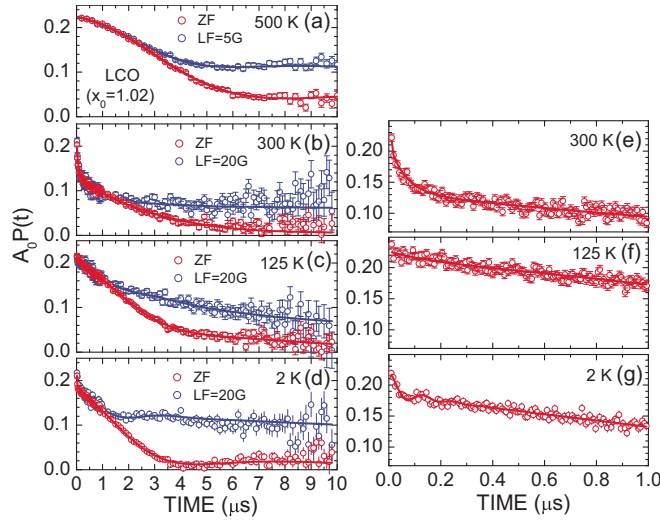
FIG. 6. (Color online) Zero-field (ZF-) and longitudinal-field (LF-) μSR spectra for the LCO($x_0 = 1.02$) sample at (a) 500, (b) 300, (c) 125, and (d) 2 K in the time domain below 10 μs. The ZF-μSR spectra in the time domain below 1 μs are also shown at (e) 300 K, (f) 125 K, and (g) 2 K. Solid lines at $125 \leq T \leq 300$ K represent the fitting results using Eq. (7), while those at 2 K are the fitting results using Eq. (9). The ZF- and LF-μSR spectra at $T \leq$ 300 K were measured at the continuous muon beam facility (PSI), while the ZF- and LF-μSR spectra at $T = 500$ K were measured at the pulsed muon beam facility (RAL).

relaxation rate by decoupling H_{int}. The ZF-μSR spectrum at 300 K exhibits a rapidly relaxing signal in the time domain below 1 μs, suggesting the appearance of magnetic phase(s) in the sample. However, since a fast relaxing signal rather than an oscillatory signal is observed in the early time domain [Fig. 6(e)], about half of the volume of the sample is found to enter into a nonordered magnetic phase. Here, we do not call this phase a disordered phase but rather a nonordered phase in order to emphasize the noble aspect of this phase.

The ZF-μSR spectrum at 125 K exhibits a KT-type relaxation, while an oscillatory signal due to the formation of AF order [12,13] is observed at 2 K together with a KT-type relaxation, i.e., a fast minimum locates at around 80 ns, and a second maximum appears at around 130 ns [Fig. 6(g)]. We therefore analyzed the ZF- and LF-μSR spectra for LCO($x_0 = 1.02$) in the two different T ranges. One is the T range between 100 and 500 K, at which the nonordered magnetic phase appears, while the other is the T range below 100 K, at which the AF-ordered phase presents. In the former T range, the ZF-μSR spectra are fitted by a combination of a dynamic Gaussian KT (DGKT) signal from a nonmagnetic phase, a fast relaxing signal from the nonordered magnetic phase, and a background (BG) signal from the muon's stopped fraction mainly in the Ag or Ti sample holder,

$$A_0 P_{ZF}(t) = A_{KT} G_{DGKT}(t, \Delta, \nu)$$
$$+ A_{fast1} \exp(-\lambda_{fast1}t) + A_{BG}, \quad (7)$$

where A_{KT}, A_{fast1}, and A_{BG} are the asymmetries associated with the three signals, λ_{fast1} is the relaxation rate, Δ is the static width of the random nuclear field, and ν is the field fluctuation
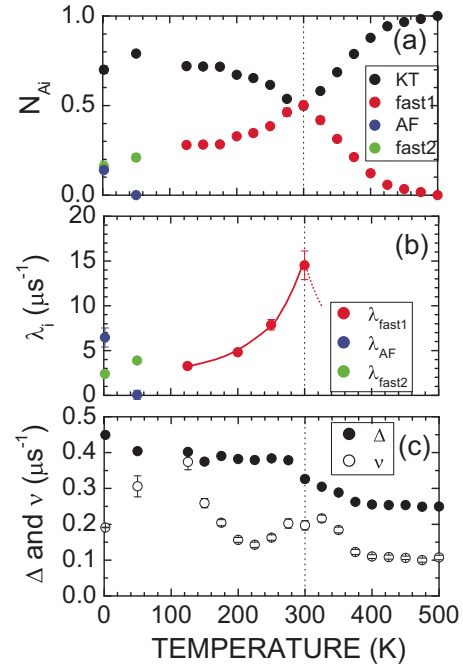
FIG. 7. (Color online) Temperature dependence of (a) normalized asymmetry N_{Ai} consisting of N_{AKT}, N_{Afast1}, N_{AAF}, and N_{Afast2}; (b) λ_{fast1}, λ_{AF}, and λ_{fast2}; and (c) Δ and ν for the LCO($x_0 = 1.02$) sample.

rate. When $\nu = 0$, $G_{DGKT}(t, \Delta, \nu)$ is a static Gaussian KT function $G_{zz}^{KT}(t, \Delta)$, given by

$$G_{zz}^{KT}(t, \Delta) = 1/3 + 2/3(1 - \Delta^2 t^2) \exp\left(-\frac{\Delta^2 t^2}{2}\right). \quad (8)$$

As reported previously [12,13], the ZF-μSR spectra at $T <$ 100 K are fitted by a combination of the oscillatory signal from the AF phase, the DGKT signal, an exponentially relaxing nonoscillatory signal due to localized moments, and the BG signal,

$$A_0 P_{ZF}(t) = A_{AF} \exp(-\lambda_{AF}t) \cos(\omega_{\mu_{AF}}t + \phi_{AF})$$
$$+ A_{KT} G_{DGKT}(t, \Delta, \nu)$$
$$+ A_{fast2} \exp(-\lambda_{fast2}t) + A_{BG}, \quad (9)$$

where A_{AF} and A_{fast2} are the asymmetries of the AF phase and disordered magnetic phase, respectively. λ_{AF} and λ_{fast2} are their relaxation rate, $\omega_{\mu_{AF}}$ ($= f_{AF} \times 2\pi$) is the muon Larmor frequency of the AF phase, and φ is the initial phase of the muon-spin precession. Note that $A_{BG} = 0$ for the μSR measurements at the PSI (continuous) facility because we used a low BG insert.

Figure 7 shows the T dependencies of the μSR-fit parameters, namely, (a) normalized asymmetries $N_{Ai} = A_i/(A_0 - A_{BG})$; (b) λ_{fast1}, λ_{AF}, and λ_{fast2}, and (c) Δ and ν. The T dependence of N_{AKT} is very similar to that of N_{ATF}, as expected. As T increases from 100 K, N_{AKT} gradually decreases, then reaches a minimum ($\sim$0.5) at 300 K, and finally increases with further increasing T. The T dependence of N_{Afast1} exhibits an opposite trend to that of N_{AKT}. At 2 K, about 14 vol% of the sample is in the AF-ordered

state with $f_{AF} = 8.4(1)$ MHz. It should be noted that the ZF-μSR measurements for Co_3O_4 revealed the presence of two oscillatory signals with $f_{AF} = 52$ and 73 MHz at 2 K with $T_N = 30$ K [22]. Also, the ZF-μSR spectrum for CoO showed the existence of three oscillatory signals with $f_{AF} = 54$, 78, and 150 MHz at 2 K with $T_N = 295$ K [27]. If we assume that the nonordered magnetism comes from the Co_3O_4 or CoO phases, N_{AF} should be ~45 vol% with $f_{AF} = 52$ and 73 MHz (or $f_{AF} = 54$, 78, and 150 MHz) at 2 K; however, as seen in Figs. 6(d), 6(g), and 7(a), $N_{AF} \sim 14$ vol% even at 2 K. Moreover, f_{AF} in LCO($x_0 = 1.02$) is quite different from those in Co_3O_4 and CoO but comparable with the previous result on ST-LCO [12,13]. Furthermore, the ZF-μSR spectrum for the OST-LCO phase, $Li_{1.04}Co_{0.96}O_{1.96}$, indicated an exponentially relaxing (nonoscillatory) signal in the time domain below 1 μs at 2 K [28]. The present ZF-μSR measurements, therefore, confirm that the nonordered magnetic phase appearing at 100 K $\leq T \leq$ 500 K is not caused by impurities, such as Co_3O_4 and CoO, but rather an intrinsic feature for ST-LCO. As T increases from 100 K, λ_{fast1} rapidly increases with T, indicating the evolution of magnitude and/or fluctuation of localized magnetic moments with T. Although it is very difficult to determine the accurate λ_{fast1} particularly above 300 K due to the limited time resolution of the pulsed muon beam, λ_{fast1} is likely to decrease with T above 300 K, as for the $N_{Afast1}(T)$ curve.

Concerning the nuclear magnetic field, as T increases from 100 K, Δ is almost T independent until 300 K, slightly decreases with T, and then keeps a constant value (~0.25 μs^{-1}) above 400 K [see Fig. 7(c)]. On the other hand, ν decreases rapidly with T up to 200 K, probably due to the effect of the AF order at low T, increases with T and reaches a maximum around 300 K, and finally decreases with T and becomes T independent above 400 K. Such behavior most likely indicates a motional narrowing due to Li diffusion around 300 K. However, the ZF and LF spectra above 400 K show a static behavior [Fig. 6(a)]. This implies that the Li ions slightly change their position around 300 K, as in the case of a cooperative Jahn-Teller transition (~285 K) in a ST-LiMn$_2$O$_4$ spinel [29]. Such a small change in the Li position would be a reason for the appearance/annihilation of the nonordered magnetic phase in ST-LCO, as discussed later.

It would be also interesting to know the situation of the delithiated LCO, i.e., $Li_{1-y}CoO_2$. Figure 8(a) shows the T dependence of N_{ATF} for the $Li_{1-y}CoO_2$ sample with $y = 0.05$ together with that for ST-LCO, i.e., LCO($x_0 = 1.02$). Although the Co^{4+} ions with $S = 1/2$ (t_{2g}^5) are produced by the delithiation reaction, N_{ATF} for the $y = 0.05$ sample maintains a value of ~1 in the T range between 75 and 300 K. This provides the firm evidence that the nonordered magnetism at ambient temperature is originated from ST-LCO solely because such electrochemical delithiation reaction does affect structural and magnetic properties of Co_3O_4 and CoO. Moreover, combining with the metallic nature of the Li-deficient LCO [9], the ZF spectrum at 300 K for the $y = 0.05$ sample indicates the absence of localized magnetic moments. Furthermore, since the ZF-μSR spectrum for the $y = 0.05$ sample indicates a dynamic KT behavior at 300 K, a slight removal of Li from ST-LCO significantly alters the nuclear magnetism of LCO due to the enhancement of Li diffusion [30].
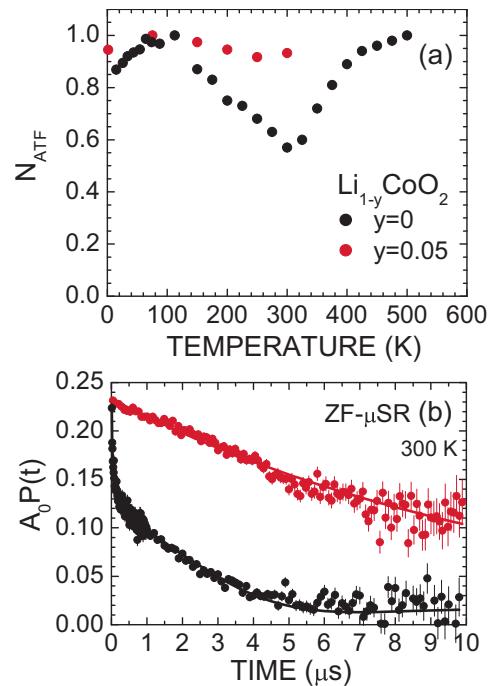
FIG. 8. (Color online) (a) Temperature (T) dependence of the normalized weak-transverse-field (wTF-) μSR asymmetry (N_{ATF}) for the delithiated $Li_{1-y}CoO_2$ sample with $x = 0.05$ and (b) its zero-field (ZF-) μSR spectrum at 300 K. The delithiated $Li_{1-y}CoO_2$ sample was prepared by electrochemical reaction using LCO($x_0 = 1.02$). T dependence of the N_{ATF} and the ZF-μSR spectrum for the initial ($y = 0$) sample at 300 K are also shown for comparison.

D. Origin of nonordered magnetism at ambient temperature

In this section we discuss a possible origin of the nonordered magnetism. We first emphasize again that the result of χ measurements looks to be inconsistent with those of EPR and μSR measurements for LCO($x_0 = 1.02$). That is, based on the χ measurements, LCO($x_0 = 1.02$) is very close to ST-LCO, suggesting that all the Co ions are in a 3+ state with $S = 0$ (t_{2g}^6). Nevertheless, the amplitude of the EPR signal for LCO($x_0 = 1.02$) is most intense among the present LCO($0.95 \leq x_0 \leq 1.10$)s. Moreover, μSR on LCO($x_0 = 1.02$) showed that the volume fraction of the nonordered magnetic phase reaches about 45 vol% at 300 K.

Here, we should note that both EPR and μSR sense static and dynamic behaviors of H_{int} with a fluctuation rate ranging from ~10^{10} Hz and 10^4–10^{12} Hz, respectively. Therefore, it is very reasonable to conclude that the Co spins in ST-LCO are fluctuating in the EPR and μSR time windows. Besides their time resolutions, we should point out a spatial resolution: μSR reflects a local magnetic environment with a few atomic distances, while χ corresponds to a macroscopic magnetism. As seen in Figs. 4(a) and 4(b), when x_0 deviates from 1.02, the intensity of the EPR signal is drastically suppressed. Furthermore, the partially delithiated sample ($Li_{1-y}CoO_2$ with $y = 0.05$), in which yCo^{4+} ions are produced, lacks localized moments above ~75 K (Fig. 8). These confirm that the localized magnetic moments at 100 K $\leq T \leq$ 500 K are strongly affected by off-stoichiometry. In other words, the ideal ST-LCO phase is found to be essential for the spin fluctuations in LCO.
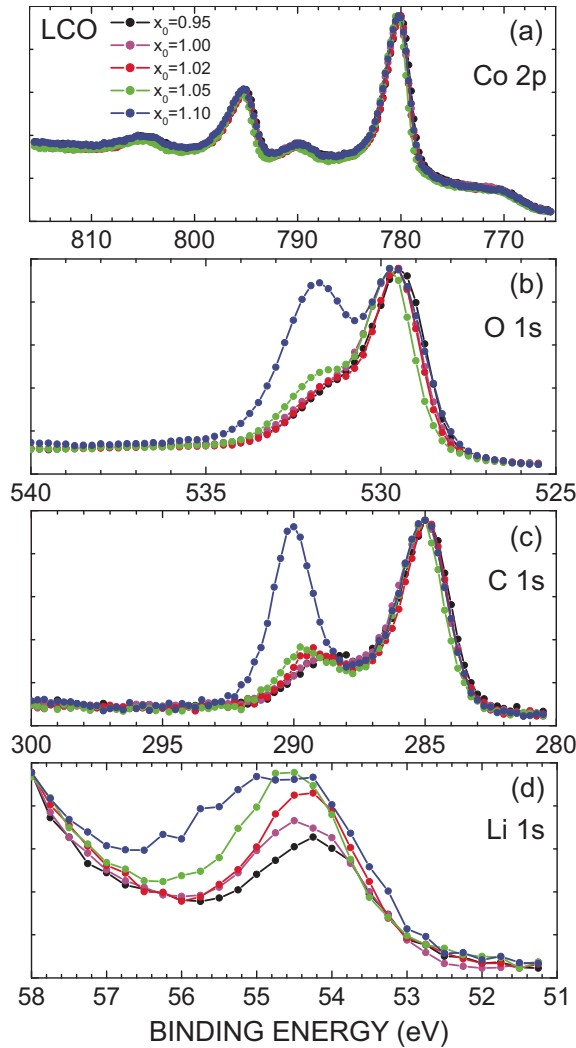
FIG. 9. (Color online) XPS spectra for the LCO($0.95 \leq x_0 \leq 1.10$) samples: (a) Co $2p$, (b) O $1s$, (c) C $1s$, and (d) Li $1s$.

According to first-principles calculations performed by Kramer and Ceder [31], the Co^{4+} ions preferentially cover the LCO surface to minimize the surface energy of LCO. In addition, Qian *et al.* [32] reported that μ_{eff}^{obs} for the nanosized ST-LCO compound increases with decreasing particle size (r) in nm with the relation of $\mu_{eff}^{obs} = 3.85/\sqrt{r}$ because the Co^{3+} ions near the surface are square pyramid or pseudotetrahedrally coordinated. However, as clarified by the XPS analyses, it is extremely difficult to rationalize the nonordered magnetism at $100\,K \leq T \leq 500\,K$ only by such surface magnetism. Figure 9 shows the XPS spectra at ambient temperature for LCO($0.95 \leq x_0 \leq 1.10$)s to obtain information on the surface. There is no detectable change in the Co $2p$ spectrum with x_0. Each spectrum consists of the Co $2p_{3/2}$ main peak at 780.1 eV with a satellite peak at 798.8 eV, and the Co $2p_{1/2}$ main peak at 795.2 eV with a satellite peak at 804.6 eV, where the intensity ratio of Co $2p_{3/2}$ to Co $2p_{1/2}$ is ~2 [Fig. 9(a)]. In contrast, making comparison with the O $1s$ main peak at 529.6 eV, a satellite O $1s$ peak at 531.8 eV clearly grows with x_0 [Fig. 9(b)]. In order to explain such an increase, Dahéron *et al.* [33] proposed the presence of oxygen deficiencies on the

OST-LCO surface using a combination of XPS analysis and *ab initio* calculations. However, the C $1s$ spectrum provides a new insight for the origin of the change in the O $1s$ spectrum with x_0 [Fig. 9(c)]. That is, a satellite C $1s$ peak at 290.1 eV also grows with x_0, particularly at $x_0 \geq 1.05$. Combining with the change in the Li $1s$ spectrum with x_0 [Fig. 9(d)], the satellite O $1s$ peak at 531.8 eV is naturally attributed to a Li_2CO_3 phase on the OST-LCO surface. Thus, although the amount of Li_2CO_3 at the surface of the LCO particle increases with x_0, the state of the Co ions does not alter with x_0.

As shown in the SEM image of LCO($x_0 = 1.02$) [Fig. 1(a)], d_{ave} is ~2 μm. Moreover, the volume fraction of the nonordered magnetic phase is ~45% at 300 K [Figs. 5 and 7(a)]. If we assume that LCO($x_0 = 1.02$) consists of spherical particles with a diameter of 2 μm and that the nonordered magnetic phase segregates at the surface of a spherical particle, the depth of the surface layer for such phase is estimated as ~180 nm, $(1 - \sqrt[3]{0.55}) \times 1000$. Since the penetration depth of a conventional XPS apparatus is ~3 nm, XPS should provide information only on such a phase. Nevertheless, the present XPS results do not show the change in the Co $2p$ spectrum but indicate the increase in the amount of nonmagnetic Li_2CO_3 phase with x_0. It should be also noted that the same XPS spectra for Co $2p$ are obtained even for the nanosized ST-LCO compound with a particle size of 10 nm [32]. This means that the Co state at the surface is not affected by both x_0 and d_{ave}. Therefore, XPS clearly excludes the possibility that the nonordered magnetism is induced by surface.

In order to reasonably explain the T dependence of N_{ATF} (or N_{Afast1}), we could consider two different factors to determine the volume of the nonordered magnetic phase. That is, one increases the volume with T, which is predominant below 300 K, while the other decreases the volume with T mainly above 300 K. One scenario is a combination of a spin-state transition and Li diffusion. A thermally induced spin-state transition is well known in $LaCoO_3$, although the exact nature of the transition is still a subject of debate [34,35]. In $LaCoO_3$, the spin-state of the Co^{3+} ions changes from an LS ground state with $S = 0$ (t_{2g}^6) to an IS excited state with $S = 1$ ($t_{2g}^5 e_g^1$) above 100 K, then alters to an HS state with $S = 2$ ($t_{2g}^4 e_g^2$) at around 500 K [35]. Assuming that such spin-state transition also occurs in ST-LCO above 100 K, the Co^{3+} ions in a thermally excited IS or HS state naturally produce localized magnetic moments. For the Co^{3+} ions in an LS state, since the triple degenerated t_{2g} orbitals are fully occupied with six d electrons, the Co^{3+} ion locates at the center of the regular CoO_6 octahedron. However, when the Co^{3+} ions are in an IS or HS state, the CoO_6 octahedron is expected to be distorted in order to minimize the total energy of d electrons. Such distortion would slightly alter the position of the Li ions, which locate around the vicinity of the distorted octahedron. At $T \geq 300\,K$, the Li ions are thought to start to diffuse between the regular $3b$ site and an interstitial site, as suggested by the $\nu(T)$ and $\Delta(T)$ curves [Fig. 7(c)]. Since the jump distance for Li diffusion is larger than the slight displacement of the Li ions from the regular site, such displacement would be suppressed with T. This also suppresses the distortion of the CoO_6 octahedron and the spin-state transition, leading to the decrease in the volume of the nonordered magnetic phase.

However, the physical properties related to a spin-state transition in LaCoO$_3$ are very different from those of LCO. For instance, χ for LaCoO$_3$ exhibits a complex T dependence below 100 K, while χ for LCO is almost T independent above 100 K, at which we assume that a spin-state transition occurs [Fig. 3(a)]. In addition, although the magnitude of the crystalline electric field splitting ($10Dq$) for LaCoO$_3$ is $\sim$0.58 eV [35], $10Dq = 2.7$ eV for LCO by XPS analyses [36]. Concerning Li diffusion, ^{7}Li-NMR observed a motional narrowing behavior due to Li diffusion around 400 K for LCO [37], which is higher by $\sim$60 K than the temperature at which the $\Delta(T)$ curve shows a gradual change for LCO($x_0 = 1.02$) [Fig. 7(c)]. Such discrepancy is likely to be explained by the difference of time resolution between NMR and μSR; however, there is still no information on the jump distance in LCO around 300 K.

The other possible mechanism is a combination between charge disproportionation of the Co^{3+} ions and Li diffusion. Since the compounds containing the Co^{4+} ions, such as CoO$_2$ and [Co$_4$O$_4$(C$_5$H$_5$N)$_4$(CH$_3$CO$_2$)$_4$]ClO$_4$, are known to exhibit a sharp EPR signal in the g range between 1.97 and 2.65 [38], the present EPR result on LCO($x_0 = 1.02$) ($g = 2.12$) implies the presence of Co^{4+} ions in an LS state with $S = 1/2$ (t_{2g}^5). Therefore, we could propose the following two charge disproportionation reactions in order to keep charge neutrality:

$$2\text{Co}^{3+}(\text{LS}, S = 0) \rightarrow \text{Co}^{2+}(\text{LS}, S = 1/2)$$
$$+ \text{Co}^{4+}(\text{LS}, S = 1/2) \qquad (10)$$

or

$$2\text{Co}^{3+} \rightarrow \text{Co}^{3+\delta} + \text{Co}^{3-\delta}. \qquad (11)$$
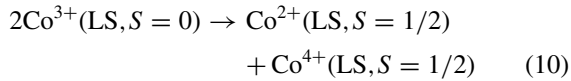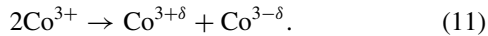
In the T range between 100 and 300 K, the reaction is thermally activated for reasons currently unknown, leading to the formation of magnetic Co^{2+} and Co^{4+} ions, while such reaction is suppressed by Li diffusion above 300 K. Note that Eq. (11) is also proposed for the related compound Na$_{0.5}$CoO$_2$ [39]. For both scenarios, magnetic Co ions should be generated with T. Hence, in order for further understanding the origin of the nonordered magnetic phase, it is highly desirable to perform careful inelastic neutron scattering studies in the T range between 100 and 500 K.

Here, we compare the present LCO result with those for Na$_{1-y}$CoO$_2$, which has a similar structure to that for LCO. Based on χ and ^{23}Na-NMR measurements on NaCoO$_2$ (NCO) [40], Co^{3+} ions are reported to be a nonmagnetic $S = 0$ (t_{2g}^6) state in the T range between $\sim$25 and 300 K. This was confirmed by μSR [41]. Thus, the past data suggest the absence of nonordered magnetism or spin fluctuation in NaCoO$_2$ [40,41].

However, stoichiometric NCO (ST-NCO) is known to be very unstable in air. In fact, the ZF-μSR spectrum for the NaCoO$_2$ sample at 1.3 K includes a fast relaxing signal with $\sim$20 vol% [41] probably due to a Co$_3$O$_4$ phase produced by decomposition of the ST-NCO [42]. This implies the possibility that the reported data was not for ST-NCO but for Na-deficient NCO. Note that the Li-deficient LCO, Li$_{1-y}$CoO$_2$ with $y = 0.05$, lacks the nonordered magnetic phase below 300 K (Fig. 8). Besides the possible Na deficiency in the NCO sample, the arrangement of the Co ions along the c axis in

ST-NCO is different from that in ST-LCO. In the former, the Co ions are located at the same (x, y) position to those in the neighboring CoO$_2$ planes due to the A-B-B-A arrangement of the O ions, whereas in the latter, the ions are at the center of the Co triangular lattice due to the A-B-B-C-C-A arrangement of the O ions. This would suggest a role of the Co-O-Na-O-Co coupling along the c axis to suppress the formation of the nonordered magnetic phase.

Finally, we point out the significance of magnetic measurements for developing LIB materials. As pointed out by Chernova *et al.* [11], it is very important to investigate physical and chemical properties of LIB materials by various experimental techniques in order to obtain a comprehensive picture of them. In fact, structural properties of LIB materials are currently studied by several techniques with different spatial resolutions, such as electron diffraction, x-ray absorption fine structure analyses, and XRD measurements. In addition, the present χ, EPR, and μSR results on ST-LCO propose the significance to employ magnetic probes with different time windows for understanding the magnetic nature. On the contrary, electrochemical properties of LIB materials have been studied in a very wide time range from 10^{-6} s to 10^7 s: a typical time-window range from 10^{-6}–10^{-3} s for polarization measurements, via 10^0–10^3 s for a quick charge and discharge cycle test, to 10^3–10^7 s for long-term charge and discharge-cycle measurements. Although there is, at present, no direct relationship between magnetism and electrochemical properties, we expect that the data on LIB materials obtained by various techniques with different spatial resolution and time windows will provide an insight for understanding the key factor to determine the performance of LIB materials.

V. CONCLUSION

We have investigated magnetic properties of LCO($0.95 \leq x_0 \leq 1.10$)s by magnetic susceptibility (χ), EPR, and muon-spin rotation and relaxation (μSR) measurements, and we found a new type of spin fluctuation in a family of layered CoO$_2$-based materials. Structural, electrochemical, and χ measurements indicated that LCO($x_0 = 1.02$) is very close to ST-LCO. However, EPR and μSR studies on LCO($x_0 = 1.02$) demonstrated the presence of local magnetic moments even at 300 K. The g value and spin–spin relaxation time T_2 of such magnetic phases were determined as 2.12(1) and 7.4(1) $\times 10^{-10}$ s, respectively. The temperature (T) dependence of wTF-normalized asymmetry (N_{ATF}) for LCO($x_0 = 1.02$) showed that as T increases from 100 to 300 K, the volume fraction of the magnetic phases increases from 0 to $\sim$45 vol% and then decreases with further increasing T and finally reaches 0 vol% at 500 K. Since the ZF μSR at 300 K exhibited a rapidly relaxing signal in the time domain below 1 μs, $\sim$45 vol% of LCO($x_0 = 1.02$) is in a nonordered magnetic phase. Considering the time window of the three techniques, the Co spins are most likely to be fluctuating in the EPR ($\sim$10^{10} Hz) and μSR (10^4–10^{12} Hz) time windows. We proposed the two possible scenarios for explaining such nonordered magnetic phase: one is a spin-state transition from an LS ground state to an IS or HS excited state, as in the case for LaCoO$_3$, and the other is a charge disproportionation reaction, $2\text{Co}^{3+} \leftrightarrow \text{Co}^{2+} + \text{Co}^{4+}$. The nonordered magnetism in ST-LCO is caused by the appearance of localized moments

because such a nonordered magnetic phase was not detected in a metallic $Li_{1-y}CoO_2$ with $y = 0.05$ sample.

[1] K. Mizushima, P. C. Jones, P. J. Wiseman, and J. B. Goodenough, Mater. Res. Bull. **15**, 783 (1980).

[2] T. Ohzuku and A. Ueda, J. Electrochem. Soc. **141**, 2972 (1994).

[3] E. Antolini, Solid State Ionics **170**, 159 (2004).

[4] K. Mukai, Y. Kishida, H. Nozaki, and K. Dohmae, Chem. Mater. **25**, 2828 (2013).

[5] S. Levasseur, M. Ménétrier, E. Suard, and C. Delmas, Solid State Ionics **128**, 11 (2000).

[6] S. Levasseur, M. Ménétrier, Y. Shao-Horn, L. Gutier, A. Audemer, G. Demazeau, A. Largeteau, and C. Delmas, Chem. Mater. **15**, 348 (2003).

[7] S. Kikkawa, S. Miyazaki, and M. Koizumi, J. Solid State Chem. **62**, 35 (1986).

[8] M. Ménétrier, A. Rougier, and C. Delmas, Solid State Commun. **90**, 439 (1994).

[9] M. Ménétrier, I. Saadoune, S. Levasseur, and C. Delmas, J. Mater. Chem. **9**, 1135 (1999).

[10] J. T. Hertz, Q. Huang, T. McQueen, T. Klimczuk, J. W. G. Bos, L. Viciu, and R. J. Cava, Phys. Rev. B **77**, 075119 (2008).

[11] N. A. Chernova, G. M. Nolis, F. O. Omenya, H. Zhou, Z. Li, and M. S. Whittingham, J. Mater. Chem. **21**, 9865 (2011).

[12] J. Sugiyama, H. Nozaki, J. H. Brewer, E. J. Ansaldo, G. D. Morris, and C. Delmas, Phys. Rev. B **72**, 144424 (2005).

[13] K. Mukai, Y. Ikedo, H. Nozaki, J. Sugiyama, K. Nishiyama, D. Andreica, A. Amato, P. L. Russo, E. J. Ansaldo, J. H. Brewer, K. H. Chow, K. Ariyoshi, and T. Ohzuku, Phys. Rev. Lett. **99**, 087601 (2007).

[14] M. Ménétrier, D. Carlier, M. Blangero, and C. Delmas, ECS Electrochem. Lett. **11**, A179 (2008).

[15] A. Artemenko, M. Ménétrier, M. Pollet, and C. Delmas, J. Appl. Phys. **106**, 064914 (2009).

[16] A. Schenck, in *Muon Spin Rotation Spectroscopy: Principles and Applications in Solid State Physics* (Adam Hilger, Bristol, 1985).

[17] G.-A. Nazri and G. Pistoia, in *Lithium Batteries: Science and Technology* (Kluwer, Dordrecht, 2004).

[18] J. Akimoto, Y. Gotoh, and Y. Oosawa, J. Solid State Chem. **141**, 298 (1998).

[19] See Supplemental Material at http://link.aps.org/supplemental/10.1103/PhysRevB.89.094406 for SM1: XRD patterns for the LCO samples, SM2: the weight fraction of the Co_3O_4 phase in the LCO sample, SM3: lattice parameters for the LCO samples, SM4: EPR spectrum for the LCO($x_0 = 1.02$) sample at 400 K, SM5: EPR spectrum of CoO at 300 K, and SM6: EPR intensity with $g = 2.12$ at 300 K as a fucntion of H_1.

[20] F. Izumi and T. Ikeda, Mater. Sci. Forum **321–324**, 198 (2000).

[21] A. Rougier, C. Delmas, and G. Chouteau, J. Phys. Chem. Solids **57**, 1101 (1996).

[22] Y. Ikedo, J. Sugiyama, H. Nozaki, H. Itahara, J. H. Brewer, E. J. Ansaldo, G. D. Morris, D. Andreica, and A. Amato, Phys. Rev. B **75**, 054424 (2007).

[23] J. S. Kim, K. W. Lee, J. J. Kweon, C. E. Lee, K. Kim, J. Lee, S. J. Noh, and H. S. Kim, Appl. Phys. Lett. **96**, 062504 (2010).

[24] R. S. Alger, in *Electron Paramagnetic Resonance: Techniques and Applications* (Interscience, New York, 1968).

[25] N. Bloembergen and S. Wang, Phys. Rev. **93**, 72 (1954).

[26] R. S. Hayano, Y. J. Uemura, J. Imazato, N. Nishida, T. Yamazaki, and R. Kubo, Phys. Rev. B **20**, 850 (1979).

[27] K. Nishiyama, S. Ohira, W. K. Dawson, and W. Higemoto, Hyp. Int. **104**, 349 (1997).

[28] J. Sugiyama, Y. Ikedo, H. Nozaki, K. Mukai, D. Andreica, A. Amato, M. Ménétrier, D. Carlier, and C. Delmas, Physca B **404**, 769 (2009).

[29] J. Sugiyama, K. Mukai, Y. Ikedo, P. L. Russo, T. Suzuki, I. Watanabe, J. H. Brewer, E. J. Ansaldo, K. H. Chow, K. Ariyoshi, and T. Ohzuku, Phys. Rev. B **75**, 174424 (2007).

[30] J. Sugiyama, K. Mukai, Y. Ikedo, H. Nozaki, M. Månsson, and I. Watanabe, Phys. Rev. Lett. **103**, 147601 (2009).

[31] D. Kramer and G. Ceder, Chem. Mater. **21**, 3799 (2009).

[32] D. Qian, Y. Hinuma, H. Chen, L.-S. Du, K. J. Carroll, G. Ceder, C. P. Grey, and Y. S. Meng, J. Am. Chem. Soc. **134**, 6096 (2012).

[33] L. Dahéron, H. Martinez, R. Dedryvère, I. Baraille, M. Ménétrier, C. Denage, C. Delmas, and D. Gonbeau, J. Phys. Chem. C **113**, 5843 (2009).

[34] S. Yamaguchi, Y. Okimoto, H. Taniguchi, and Y. Tokura, Phys. Rev. B **53**, R2926 (1996).

[35] M. A. Korotin, S. Yu. Ezhov, I. V. Solovyev, V. I. Anisimov, D. I. Khomskii, and G. A. Sawatzky, Phys. Rev. B **54**, 5309 (1996).

[36] J. van Elp, J. L. Wieland, H. Eskes, P. Kuiper, G. A. Sawatzky, F. M. F. de Groot, and T. S. Turner, Phys. Rev. B **44**, 6090 (1991).

[37] K. Nakamura, H. Ohno, K. Okamura, Y. Michihiro, T. Moriga, I. Nakabayashi, and T. Kanashiro, Solid State Ionics **177**, 821 (2006).

[38] J. G. McAlpin, T. A. Stich, C. A. Ohlin, Y. Surendranath, D. G. Nocera, W. H. Casey, and R. D. Britt, J. Am. Chem. Soc. **133**, 15444 (2011).

[39] K.-W. Lee, J. Kuneš, and W. E. Pickett, Phys. Rev. B **70**, 045104 (2004).

[40] C. de Vaulx, M.-H. Julien, C. Berthier, M. Horvatic, P. Bordet, V. Simonet, D. P. Chen, and C. T. Lin, Phys. Rev. Lett. **95**, 186405 (2005).

[41] G. Lang, J. Bobroff, H. Alloul, P. Mendels, N. Blanchard, and G. Collin, Phys. Rev. B **72**, 094404 (2005).

[42] P. Mendels (private communication).